Enzyme-Catalyzed Spiroacetal Formation in Polyketide Antibiotic Biosynthesis

Oksana Bilyk[a]†[*] , Gabriel S. Oliveira[b], Rafaela M. de Angelo[c], Michell O. Almeida[d], Kathia Maria Honório[c], Finian J. Leeper[e] , Marcio V. B. Dias[b,f*], and Peter F. Leadlay[a]

[a] Department of Biochemistry, University of Cambridge, 80 Tennis Court Road, Cambridge, CB2 1GA, UK,

[b] Department of Microbiology, Institute of Biomedical Science, University of Sao Paulo, Av. Prof. Lineu Prestes, 1374, São Paulo, SP, 05508-000, Brazil.

[c] School of Arts, Sciences and Humanities (EACH), University of Sao Paulo, São Paulo, SP, 03828-000, Brazil.

[d] Institute of Chemistry of Sao Carlos (IQSC), University of Sao Paulo, Sao Carlos, SP, 13566-590, Brazil.

[e] Yusuf Hamied Department of Chemistry, University of Cambridge, Lensfield Road, Cambridge, CB2 1EW, UK.

[f] Department of Chemistry, University of Warwick, Coventry, CV47 7AL, UK.

Corresponding authors:

*O.B: e-mail: oksana.bilyk@recircle.com

*M.V.B.D.: email: mvbdias@usp.br

Present Addresses

†O.B: Recyclatech Group Ltd., Octagon Point, 5 Cheapside, London, EC2V 6AA, UK.

Keywords: •polyketides • spiroacetals • spirocyclases • biosynthesis • calycin protein family

ABSTRACT: A key step in the biosynthesis of numerous polyketides is the stereospecific formation of a spiroacetal (spiroketal). We report here that spiroacetal formation in the biosynthesis of the macrocyclic polyketides ossamycin and oligomycin involves catalysis by a novel spiroacetal cyclase. OssO from the ossamycin biosynthetic gene cluster (BGC) is homologous to OlmO, the product of an unannotated gene from the oligomycin BGC. Deletion of *olmO* abolished oligomycin production and led to the isolation of oligomycin-like metabolites lacking the spiroacetal structure. Purified OlmO catalyzed complete conversion of the major metabolite into oligomycin C. Crystal structures of OssO and OlmO reveal an unusual 10-strand β-barrel. Three conserved polar residues are clustered together in the β-barrel cavity, and site-specific mutation of any of these residues either abolished or substantially diminished OlmO activity, supporting a role for general acid/general base catalysis in spiroacetal formation.

INTRODUCTION

The specialized polyketide metabolites produced by *Streptomyces* and allied bacteria constitute an impressive natural pool of potential drugs and drug leads.[1,2] This chemical diversity is due in large part to the action of specific cyclases and other auxiliary enzymes that act on the initial products of polyketide chain assembly.[3-5] A particularly striking feature of a number of complex polyketides is the presence of a 6,6-spiroacetal (also referred to as a 6,6-spiroketal) moiety,[6-9] as shown in Figure 1 for the cytotoxic compounds oligomycin **1** and ossamycin **2**. The configuration of the spiro carbon in natural polyketide metabolites is almost invariably that predicted to be the most thermodynamically stable, taking into account both steric effects and anomeric effects.[7] Until fairly recently, therefore, it was a tenable hypothesis that spiroacetal formation is a late-stage non-enzyme-catalyzed process in polyketide biosynthesis.

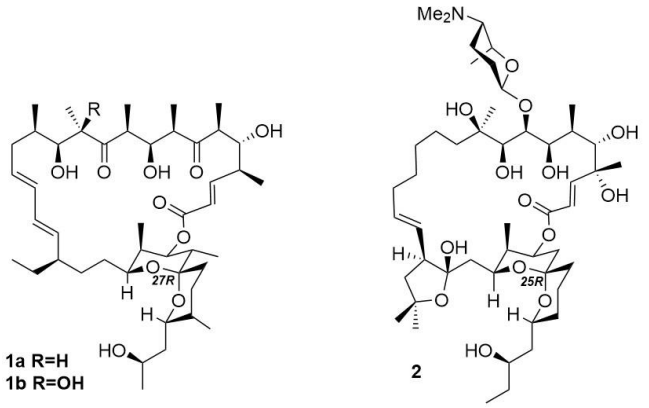

Figure 1. Cytotoxic macrocyclic spiroacetals. The structures of oligomycin C (**1a**), oligomycin A (**1b**) and ossamycin (**2**).

The first evidence for the existence of specific spirocyclase enzymes came from the examination of the biosynthetic pathway to the cell cycle inhibitor reveromycin A.[10] In the presence of spirocyclase RevJ, dehydrative cyclization of an acyclic 11,19-dihydroxy-15-ketone precursor gave the natural (15*S*) configuration of reveromycin; while in its absence, non-enzymatic cyclization yielded a mixture of (15*R*) and (15*S*) isomers. Similarly, in the biosynthetic pathway in *Streptomyces avermectinius* to the antiparasitic compound avermectin,[11] AveC is required for the stereospecific spiroacetalization of a C17, C25-dihydroxy C21-ketone polyketide precursor to yield the 21*R* configuration at the spiro atom. A third example is the putative spirocyclase SalE/SlnM in the pathway to the polyether ionophore salinomycin A.[12,13] There is no sequence similarity between RevJ, AveC and SalE/SlnM, and it appears that spirocyclase enzymes have independently evolved several times (Supplementary Figure 1). No crystal structure has been determined for any of these enzymes.

We recently identified OssO, in the biosynthetic gene cluster for the 24-membered macrocyclic polyketide ossamycin from *Streptomyces ossamyceticus* as a putative spirocyclase,[14] on the basis that phylogenetic analysis showed significant sequence similarity between OssO and several other proteins, each associated with a polyketide biosynthetic gene cluster, one of which is the product of the unidentified gene *olmO* in the gene cluster for the spiroacetal oligomycin.[15] We show here that OlmO and OssO are indeed representatives of a newly-recognized spirocyclase family, having no sequence similarity either to RevJ, AveC or SalE/SlnM; and on the basis of their crystal structures and the results of site-specific mutagenesis of OlmO, we suggest a catalytic mechanism for spiroacetal formation.

RESULTS AND DISCUSSION

Deletion of Putative Spirocyclase Genes *ossO* and *olmO*.

To assess the role of *ossO* in the biosynthesis of ossamycin, the gene was deleted in-frame from the *S. ossamyceticus* chromosome using inactivation plasmid pYH7[16] carrying 2-kbp regions of flanking DNA, as previously described (Supplementary Figure 2).[14] The correctness of the deletion was confirmed by PCR analysis and DNA sequencing. However, there was no difference, as judged by HPLC-linked mass spectrometry, between the metabolites in crude extracts from the wild-type strain and from *S. ossamyceticus* Δ*ossO*, apart from a slight decrease in production levels. The presence of OssO is not essential *in vivo* for spirocyclization of ossamycin, presumably because of a non-enzymatic ring closure under these conditions (Supplementary Figure 2c).

In contrast, deletion of *olmO* from *Streptomyces avermectinius* very significantly reduced oligomycin production. Inactivation of *olmO* was carried out in the avermectin-producing strain *S. avermectinius* VL1001.[11] The gene was inactivated via a double crossover event and the integrity of the Δ*olmO* in-frame deletion mutant (*S avermictinius* Δ*olmO*) was confirmed by PCR analysis and sequencing (Supplementary Figure 2b). LC-ESI-MS analysis of extracts from the culture medium of the mutant showed the presence of only minor amounts of oligomycin C (12-deoxyoligomycin A) **1a** (*m/z* 797.5174 $[M+Na]^+$) (approx. 5% of wild-type levels) (Figure 2). *In trans* complementation of the mutant with a copy of *olmO*, supplied on a plasmid vector and transcribed from the constitutive *ermE** promoter, fully restored oligomycin production. Expression of *ossO* under the same conditions had no effect, suggesting high substrate specificity of these enzymes (Figure 2). Analysis of the extracts from the Δ*olmO* mutant showed the appearance of two new metabolites, the major one **3a** (*m/z* 815.5280 $[M+Na]^+$) eluting at 15 min, and the minor one **3b** (*m/z* 831.5229 $[M+Na]^+$) eluting at 12.5 min (Figure 2).

The difference from the ossamycin case, where non-enzymic spirocyclization seems to occur, may be because **3a** is slower to cyclize non-enzymically due to steric hindrance from the extra methyl groups on the spirocyclic rings of **1a**.

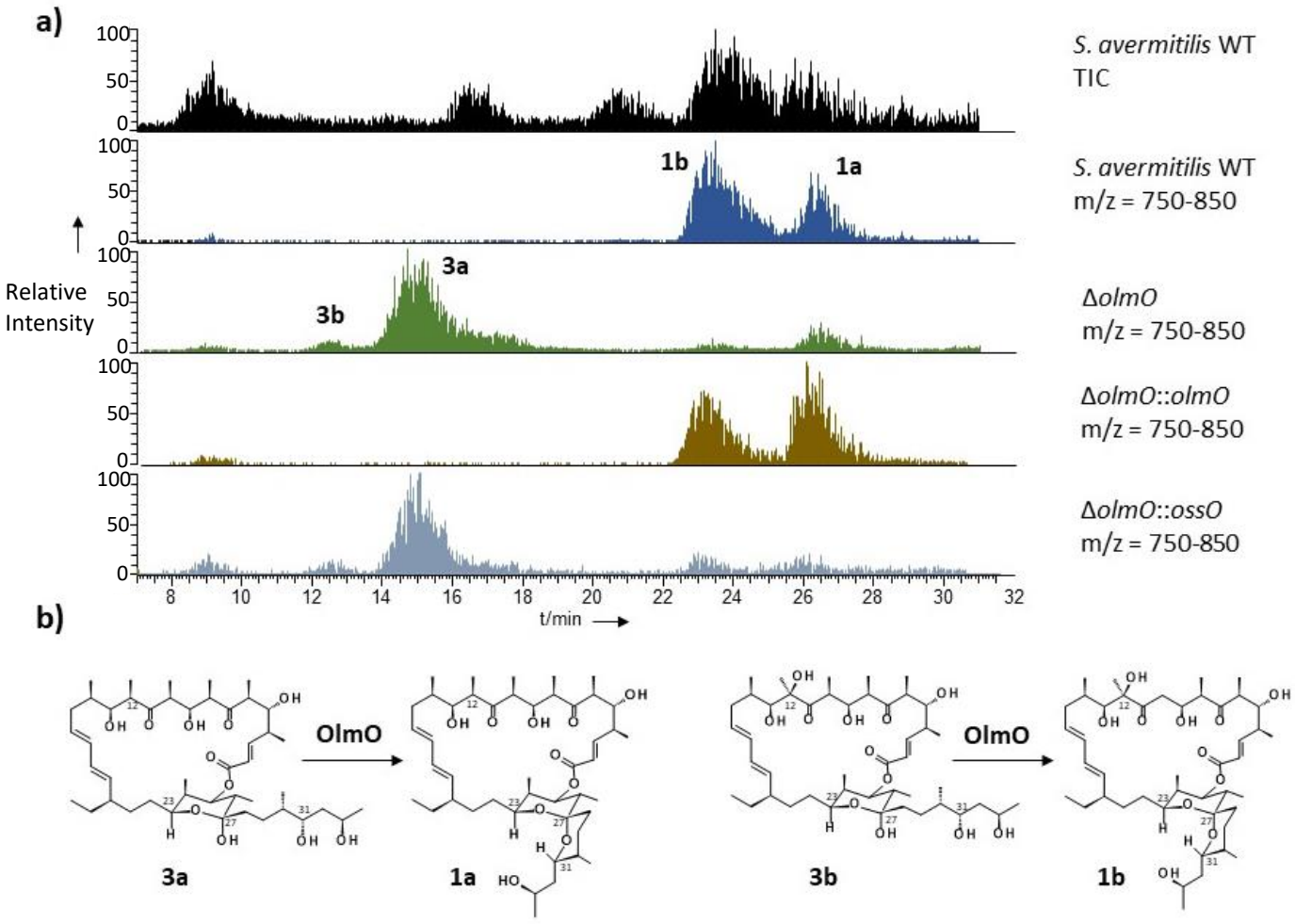

Figure 2. Functional characterization of spirocyclase OlmO in oligomycin biosynthesis. a) HPLC-MS analysis of the production of oligomycin C **1a** (*m/z* = 797.5174 $[M+Na]^+$) and oligomycin A **1b** (*m/z* = 813.5123 $[M+Na]^+$), and of hemi-acetals of oligomycin C **3a** (*m/z* = 815.5280 $[M+Na]^+$) and oligomycin A **3b** (*m/z* = 831.5229 $[M+Na]^+$), from *S. avermectinius* VL1001 (wild type (WT)), a *S. avermectinius* VL1001 gene deletion mutant, and the deletion mutant complemented with either OlmO or OssO. Data representative of three independent experiments. **b)** The proposed role of the OlmO spirocyclase in oligomycin biosynthesis.

OlmO Catalyzes Spiroacetal Formation *in vitro*.

Optimization of the purification conditions and reduced handling time enabled substantial purification of both **3a** and **3b** in yields of 8.1 mg and 2.4 mg respectively, starting from 6 L of fermentation medium. In the presence of trace amounts of formic acid **3a** and **3b** were completely converted into **1a** and **1b**, respectively, as expected of hemiacetal analogues of oligomycin C and A (Supplementary Figure 3). High-resolution mass analysis of **3a** gave the formula $C_{45}H_{76}O_{11}$ with a molecular ion of *m/z* 815.5274 (calc. *m/z* 815.5280 $[M+Na]^+$, Supplementary Figure 4). The observed mass corresponds precisely to that expected for a hemiacetal of oligomycin C (Figure 2), with five hydroxy groups present instead of the four in oligomycin C. High-resolution mass analysis of **3b** gave the formula $C_{45}H_{76}O_{12}$ and a molecular ion of *m/z* 831.5225 (calc. 831.5229 $[M+Na]^+$, Supplementary Figure 5) corresponding to a hemiacetal form of oligomycin A. These results clearly established the identity of **3a** and **3b** as oligomycin hemiacetals. This suggests that formation of the spiroacetal is not required for hydroxylation at C-12.

NMR analysis of **3a** was also undertaken, to gain information about the predominant form of the hemiacetal, and in particular, which of the rings that will form the spiroacetal remains open. The NMR spectra obtained (Supplementary Figures 6-9, Supplementary Table 2 and Supplementary Note 2) closely resembled those of oligomycin A as a reference (Supplementary Figure 6, Supplementary Table 1 and Supplementary Note 1), the obvious differences being attributable to a significant fatty acid impurity remaining in the sample of **3a**; and to expected differences due to the additional

-OH at C-12 in oligomycin A. There are some further differences possibly due to one of the rings of the acetal being open, but these are difficult to interpret. One clear observation however is that the couplings to the H next to the ester oxygen (H-25) at ~5.00 ppm are the same in **3a** and in oligomycin A (dd, J = 5.0 and 11.3). The large 11.3 Hz coupling is to H-26 in oligomycin A and is expected because H-25 and H-26 are both axial and *trans* to each other; and since the same large coupling is observed in the sample of **3a**, it suggests that these protons are also in a six-membered ring, meaning that the predominant form of the hemiacetal has the other ring open (C-27 to C-31) (Supplementary Figure 10).

Putative spirocyclases OlmO and OssO were overexpressed in *Escherichia coli* and purified using metal ion affinity and anion exchange column chromatography. Freshly purified **3a** and **3b** were incubated with either OlmO or OssO (each at 5 μM) at 30 °C for 1 h. Assays in which OlmO was present showed complete conversion of **3a** into **1a** and of **3b** into **1b** (Figure 3, Supplementary Figure 11). In contrast, in the presence of OssO, **3a** showed less than 1% conversion into **1a** (Figure 3).

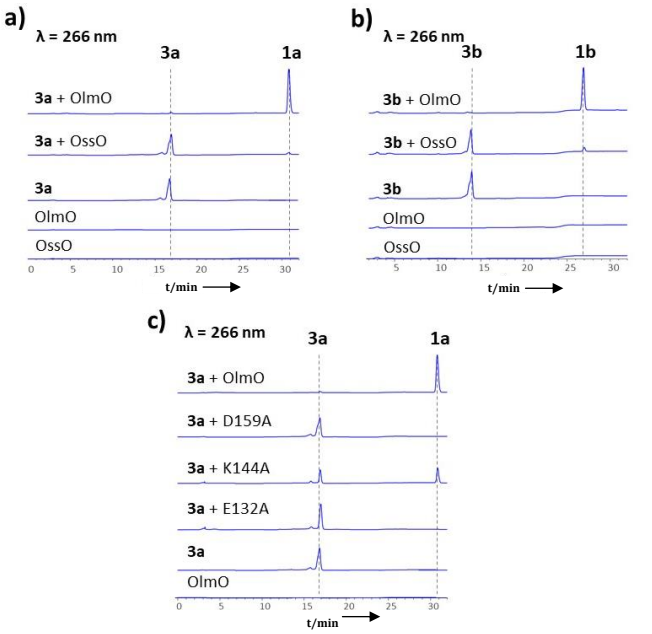

Figure 3. Spirocyclase activity of OlmO *in vitro*. **a)** conversion of hemiacetal **3a** into oligomycin C **1a. b)** conversion of hemiacetal **3b** into oligomycin A **1b**. OssO showed little or no spirocyclase activity against oligomycin substrates. **c)** conversion of hemiacetal **3a** into oligomycin C **1a** by wild-type OlmO and by site-specific mutants of OlmO. The y-axis represents the relative intensity (%)

OlmO- and OssO-Related Enzymes Represent a New Enzyme Family.

BLAST searches[17] of public databases uncovered numerous sequences of proteins, from *Streptomyces* or closely allied genera, with significant sequence similarity to OlmO and OssO. The multiple sequence alignment[18] of 28 of these proteins with OlmO and OssO is shown in Supplementary Figure 12, and a phylogenetic tree[19] is shown in Figure 4. The genomic context of each gene was also analyzed and compared with the gene arrangement in well-characterized biosynthetic gene clusters. In almost all cases, the candidate spirocyclase was found associated with neighboring genes for modular polyketide synthase multienzymes, and with auxiliary genes typical of specific classes of complex polyketide.

A total of seven spirocyclase candidates grouped phylogenetically with OssO (Figure 4) and were found encoded in ossamycin-like gene clusters, although the exact products encoded by those clusters remain to be identified. Likewise, all hypothetical and candidate spirocyclases whose sequences grouped with OlmO were found in oligomycin-like clusters. Intriguingly, the three oligomycin-like clusters most closely resembling the authentic oligomycin cluster of *S. avermectinius* (formerly *S. avermitilis*)[15] are also flanked by a set of genes encoding the F0F1-ATP synthase, the target of inhibition by oligomycin in eukaryotic cells. A further member of this subgroup of spirocyclases (AOS63731.1) is found within an oligomycin-like modular PKS gene cluster in the fully-sequenced genome of the marine sponge-associated actinomycete *Actinoalloteichus hymeniacidonis*.[20] The product of this cluster is unknown, but scrutiny of the sequence suggests the use of more than one type of unusual extender unit in the polyketide chain, which is the hallmark of the oligomycin-like neomaclafungins previously reported from the marine strain *Actinoalloteichus* sp. NPS702A. [21]

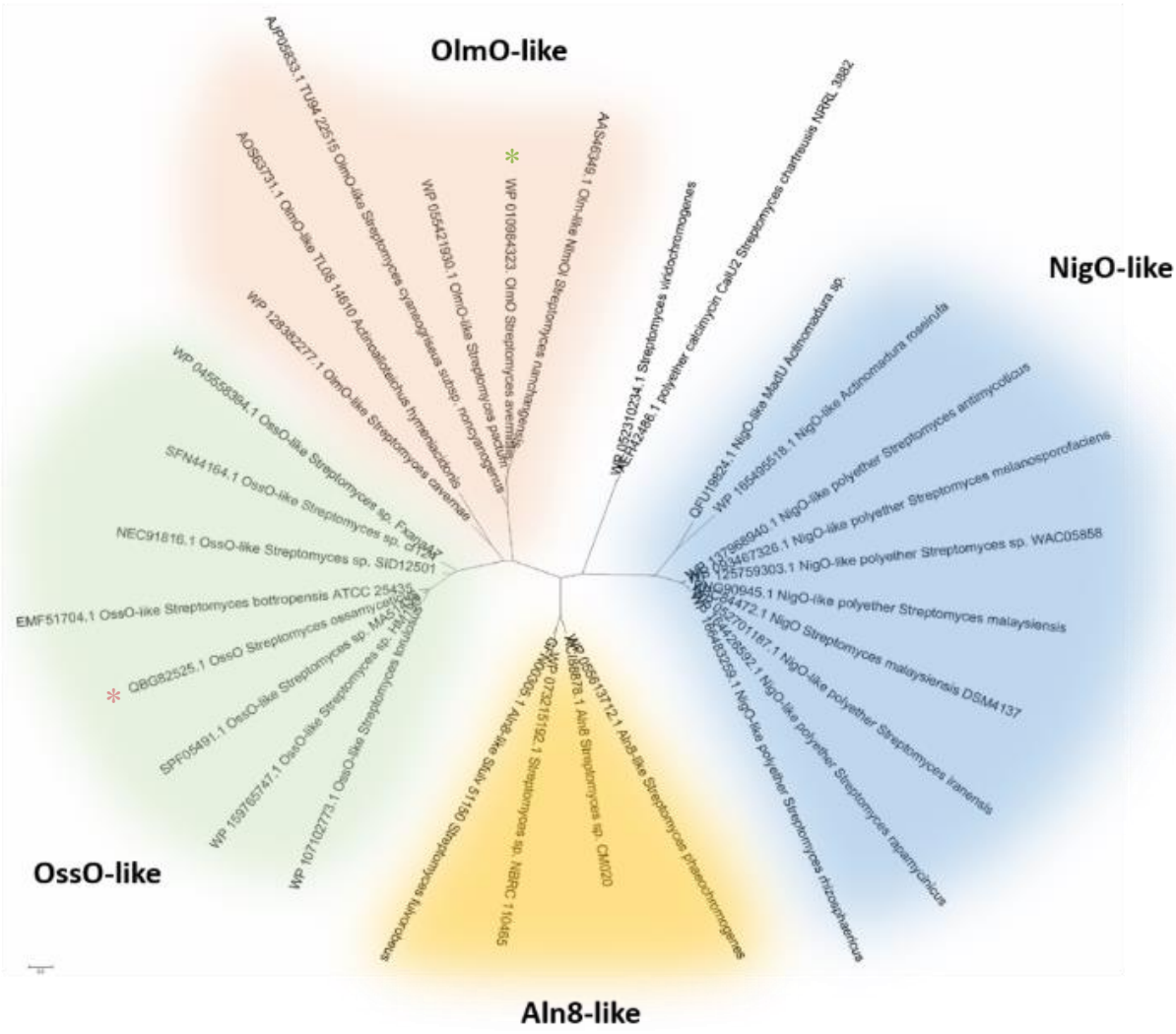

Figure 4. Phylogenetic tree of spirocyclases in the OlmO/OssO structural family. The sequences of 28 hypothetical candidate spirocyclases were obtained from public databases and compared with OlmO and OssO. The maximum-likelihood tree demonstrates the existence of distinct clades of spirocyclases: OssO-like spirocyclases are highlighted in green, OlmO-like in pink, NigO-like in blue, Aln8-like in yellow (Some of the enzymes, *e.g.* NigO, are hypothesized to catalyze the production of a 6,5-spiroacetal moiety instead a 6,6-system. Names with asterisks in the green and salmon areas are the strains and sequences for OssO and OlmO, respectively.

Other spirocyclases that group phylogenetically with NigO (formerly ORF9) from the biosynthetic gene cluster for the [6,5]-spiroacetal-containing polyether ionophore nigericin[22] are found in polyether gene clusters also predicted to produce nigericin or a close analogue. One such NigO-like enzyme, MadU, is located in a known gene cluster in *Actinomadura* sp. J1-007 for production of the [6,5]-spiroacetal-containing polyether antibiotic maduramicin.[23] Several putative spirocyclases were identified related to Aln8, a protein of unknown function from the alnumycin biosynthetic pathway in *Streptomyces* sp. CM020.[24] Alnumycin is an isochromanequinone polyketide antibiotic structurally related to actinorhodin, which features a highly unusual acetal in the form of a 4-hydroxymethyl-5-hydroxy-1,3-dioxan moiety. It seems plausible that Aln8 might play a hitherto-unsuspected role in the final step of acetal formation.[25, 26] Another OlmO/OssO homologue is the product of the uncharacterized *schU2* gene from the biosynthetic gene cluster of *Streptomyces chartreusis* governing the production of the pyrrole polyether antibiotic calcimycin (A23187).[27] SchU2 may likewise play a role in the formation of the spiroacetal of calcimycin. These findings, taken together, suggest that enzyme-controlled spiroacetal formation is a widespread feature in polyketide antibiotic biosynthesis, rather than being restricted to specific examples

of [6,6]-spiroacetal formation. Apart from the obvious catalytic benefit of accelerating the formation of a single stereoisomer, and of suppressing side-reactions of the initially-formed polyketide chain, it is conceivable that acquisition of a spiroacetal synthase activity during evolution might be a key step in diverting an existing biosynthetic pathway to produce a radically different structure.[28]

OlmO and OssO Crystal Structures reveal a calycin-like β-Barrel Fold.

While OlmO and OssO have an identity of about 40%, the sequence alignment of all the spirocyclase candidates in Supplementary Figure 12 shows that there is considerable variation in their N-termini, but also several regions of very high sequence similarity. For example, there is an almost wholly conserved sequence (D,E,Q)LDFLLG at residues 27-33 (OlmO numbering); and another conserved sequence motif YYDDWG at residues 95-100. The proteins in the NigO clade all have an additional 10 amino acids inserted between residues 123 and 124 of OlmO. To gain further insight into the structure and function of these enzymes, we have determined the crystal structure of both OlmO and OssO and deposited them in the Protein Data Bank with the entries 7SFN and 7SFP, respectively.

Recombinant OlmO and OssO behaved as homodimeric proteins in gel filtration, and for OlmO sedimentation velocity experiments indicated a homodimer of 42.5 kDa (Supplementary Figure 13). The X-ray crystal structures of both OlmO and OssO were determined in their *apo* form at a resolution of 2.1 and 2.2Å resolution, respectively (Supplementary Table 3). The asymmetric unit of OlmO crystals contains two protomers, corresponding to the homodimeric quaternary structure observed in solution. OssO has a single protomer, but the corresponding dimer can be readily obtained using crystallographic symmetric operations. The spirocyclases have 43% amino acid sequence identity and the main chains superimpose with an r.m.s.d. of 1.12Å (Supplementary Figures 14 and 15, respectively). Both structures consist of a ten-stranded antiparallel β-barrel capped by a 3_{10} α-helix at one end, while the other end is solvent-exposed (Figure 5). Electron density maps were well-defined and gave rise to good-quality models as judged using Molprobity[29], except for the N-termini (residues 1-15 for OlmO, 1-25 for OssO) and for residues 123-128 in OlmO (Supplementary Figure 16). The dimer interface in both OlmO and OssO is formed by hydrophobic interactions of residues in β-strands β4-β6, positioned back-to-back with the adjacent subunit (Supplementary Figure 17), so dimerization does not obstruct access to the interior of the barrel.

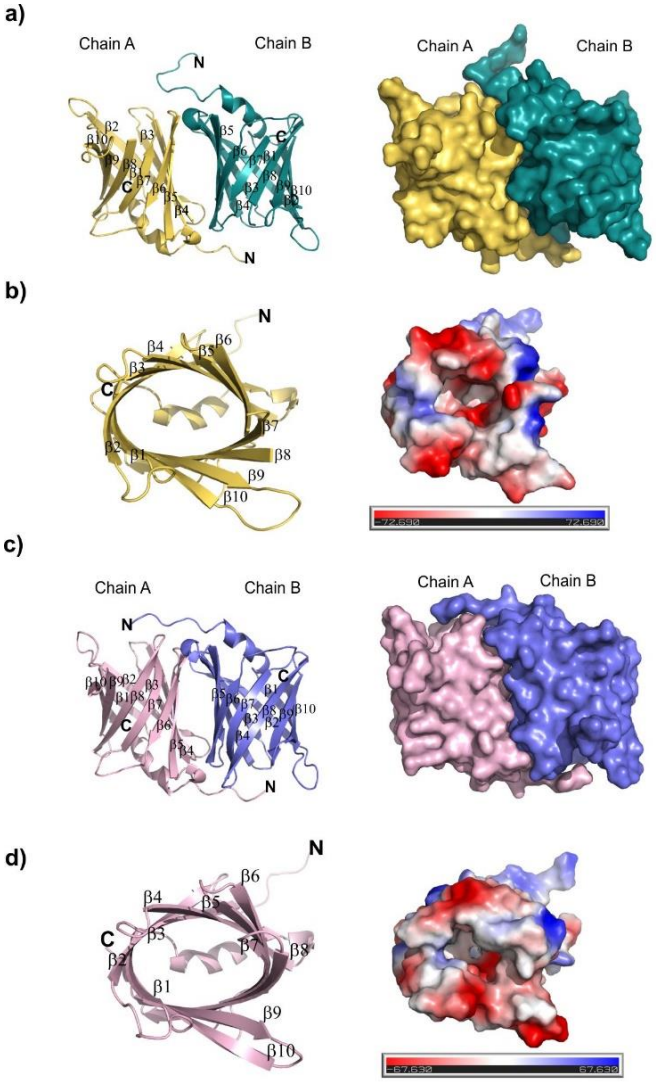

Figure 5. The overall structure of spirocyclases. **a)** Ribbons and surface representation of OlmO. Each colour represents a different subunit. **b)** the cavity within the 10 stranded β-barrel, viewed from the open end, in ribbons and electrostatic potential surface. **c)** Ribbons and surface representation of OssO. Each colour represents a different subunit. **d)** the cavity in OssO, viewed from the open end, represented in ribbons and electrostatic potential surface. The surface charge was calculated using PyMOL (PyMOL Molecular Graphics System, Schrödinger, LLC) and is represented in eV^{-}. Blue represents positive charge and red negative charge.

Surprisingly, a search using either OlmO or OssO as a probe against the DALI server[30] returned structures of proteins in the calycin superfamily, comprising lipocalins and fatty acid binding proteins (FABPs). These proteins are involved in recognition, transport, or storage of diverse small molecules.[31, 32] They show

no sequence homology to OlmO or OssO although they feature the same antiparallel β-barrel surrounding a hydrophobic cavity, closed at one end by a 3_{10} α-helix (Supplementary Figure 18). The mammalian lipocalin-type prostaglandin D synthase is one of only a few enzymes known to adopt similar scaffold.[33]

Structural Comparison of OssO and OlmO

The superimposition of OlmO and OssO shows that these enzymes have most elements of secondary structure conserved (Figure 5 and Supplementary Figure 15). The highly conserved region 28-LDFLLG-33 (OlmO numbering) noted in all analyzed spirocyclase sequences (Supplementary Figure 12) lies at the start of the β1 strand of the β-barrel, and other conserved residues are also concentrated in β strands. The major differences in the Cα-traces of OlmO and OssO are seen in the loops between β7 and β8, and between β9 and β10 (Figure 5 and Supplementary Figure 15). In OlmO, these regions adopt a more open and flexible conformation and the loop between β7 and β8 does not show clear electron density. In addition, the β-turn between the β3 and β4 strands in OlmO has a more open conformation than in OssO and it is shifted by about 1.9Å (Supplementary Figure 15). The lumen of the β-barrel of OlmO and OssO provides a large and deep cavity for the spirocyclase active site. Its volume was calculated, using the webserver CASTp 3.049,[34] as 350Å^3 and 513Å^3 for OssO and OlmO, respectively (Supplementary Figure 19). The specific size and shape of the cavity for each enzyme is defined by different sets of residues with bulky hydrophobic sidechains: Trp39, Trp54, Phe80, Leu105, Phe117, Phe128 and Leu130 in OlmO (Supplementary Figure 18A); and Tyr50, Leu78, Trp91, Phe116, Phe135, Phe141 and Phe145 in OssO (Supplementary Figure 20B). However, OlmO/OssO also have a number of conserved polar and charged residues, including Asn41/52, Thr43/54, Gln69/80, Tyr95/106 and Asp97/108; and those previously observed in the multiple sequence alignment, including Glu132/143, Lys144/155 and Asp159/169 (Supplementary Figure 20C-D), located in the β8, β9 and β10 strands, respectively. The latter two residues are fully conserved in all 14 sequences in OlmO and OssO clades, while Glu132/143 is conserved in all except four where it is conservatively replaced by Asp (Supplementary Figure 12). The two acidic sidechains are close enough that they both form an ionic interaction with the lysine sidechain (Figure 6). We considered this conserved cluster of polar residues, on the same side of the β-barrel cavity, as possible participants in the catalytic mechanism of the spirocyclase. To investigate this, we undertook docking, molecular dynamic simulations and site-directed mutagenesis. Docking simulations were performed using OlmO as receptor and **3a** as ligand. We observed that **3a** fits well in the OlmO active site, as judged by complementarity of shape and charge and the formation of the expected hydrogen bonds of carboxyl groups of Asp159 and Glu132 with the C27-hydroxyl and the C31-hydroxyl groups from **3a**, respectively (Figure 6C-D and Supplementary Figure 21). To validate the docking results, we have performed a molecular dynamic simulation with a time interval of 100 ns for both apo enzyme and the OlmO:**3a** complex. r.m.s.d. and r.m.s.f. plots for the trajectories were generated (Supplementary Figure 22 and supplementary note for energy analysis of molecular dynamics). The r.m.s.d. for OlmO in apo form showed a higher variation during the simulation compared to the OlmO:**3a** complex. However, the protein-substrate complex has a higher r.m.s.d. indicating greater flexibility. Even so, the r.m.s.d. for the OlmO:**3a** complex showed a greater stability during the simulation in those subtrajectories which supports the catalytic mechanism proposed below. On the other hand, the r.m.s.f. analysis (Supplementary Figure 22) indicates that there are regions of high fluctuations that are expected to occur, including loop regions of the extremity of the β-barrel. However, the analysis of hydrogen bond formation and the r.m.s.f. plot also indicated that the charged residues, particularly Glu132, Asp159, and Lys144 (which correspond to the positions 116, 143, and 128 in the plot of Supplementary Figure 22c, respectively), stay in close contact and forming hydrogen bonds during the molecular dynamic trajectories (Supplementary Figure 22d-f), strongly suggesting that these residues participate in the spirocyclization reaction.

Evidence for General Acid-General Base Catalysis at the Active Site of Spirocyclase OlmO.

Based on the results of structural analysis, molecular docking and molecular dynamics simulations, site-directed mutagenesis was used to mutate each of Glu132, Lys144 and Asp159 to alanine, as described in the Methods section (Supplementary Material). All three mutated enzymes were expressed in *E. coli* as soluble proteins at levels similar to the wild-type protein. The purified proteins were tested for their ability to convert **3a** into **1a** in *in vitro* assays. Alteration of either

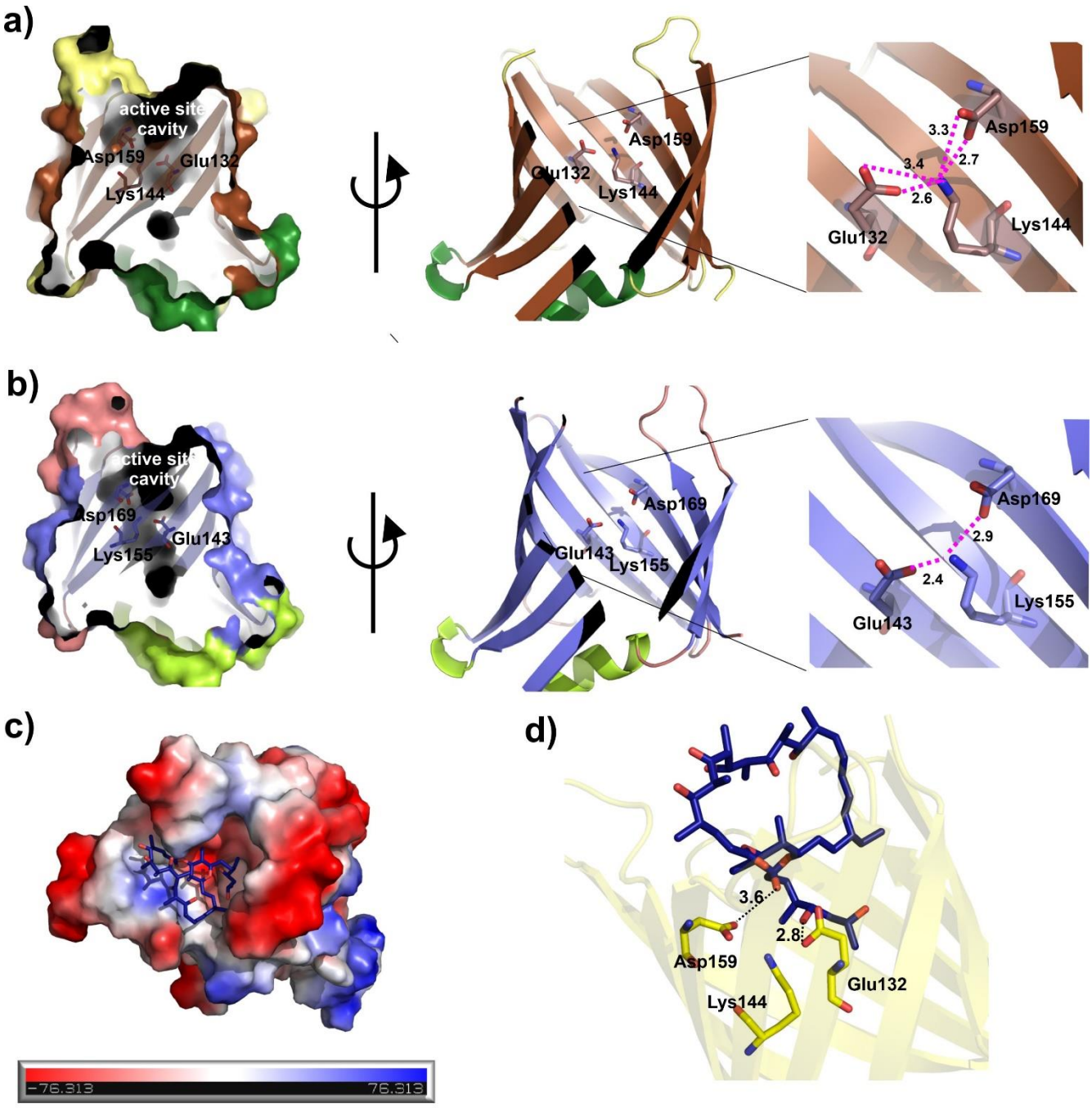

Figure 6. Spirocyclase active site. **a)** OlmO. The left and central figures show a section through the barrel from the side and the location of a proposed cluster of active site residues. The distances (in Å) between these residues are shown on the right. **b)** OssO. The figures are as in **a)**, showing the conserved arrangement of the active site between OssO and OlmO. **c)**, representation of electrostatic potential surface for OlmO with the proposed docking position of **3a.** Regions in blue, red, and white have positive, negative and neutral charges, respectively. **d)**, the interaction of **3a** with OlmO based on docking simulation. **3a** is represented with the carbons in dark blue and the amino acids proposed to be involved in the catalysis are presented with carbons in yellow.

Glu132 or Asp159 to Ala gave wholly inactive enzymes, while alteration of Lys144 to Ala markedly reduced enzyme activity with only 50% conversion being observed (Figure 3C). These findings support a role for these conserved acidic residues in catalysis. In the conversion of oligomycin hemiacetal **3a** into oligomycin C **1a (**Figure 7) Asp159 may assist as a general acid in the initial dehydration to form the oxocarbenium ion, while Glu152 (as the carboxylate anion) may then assist as a general base in the subsequent nucleophilic attack by the C-31 hydroxy group to form the spiroacetal.

CONCLUSION

In summary, we have functionally and structurally characterized the unprecedented spirocyclases OlmO and OssO involved in the biosyntheses of oligomycin and ossamycin, respectively. The sequence analysis of these proteins indicates that numerous natural products containing spiroacetal ring systems might rely on enzymatic strategies as similar genes with undefined functions are present in their BGCs, including polyether ionophore antibiotics, such as calcimycin and nigericin. The crystal structures of OlmO and OssO reveal a calycin-like fold, which is common for eukaryotic proteins involved in the binding and transport of liposoluble small molecules[31], but not usually described for enzymes. The unique enzyme previously identified as using a similar calycin-like barrel to house its active site is the mammalian lipocalin-type prostaglandin D synthase.[33] However, PGDS has an entirely unrelated catalytic mechanism, dependent on an activated cysteine and the formation of an S-O adduct.[35] The mechanism delineated here for OlmO and OssO is unprecedented for this calycin protein family, and provides fresh insight into enzymatic strategies for the construction of spiroacetal moieties in natural products.

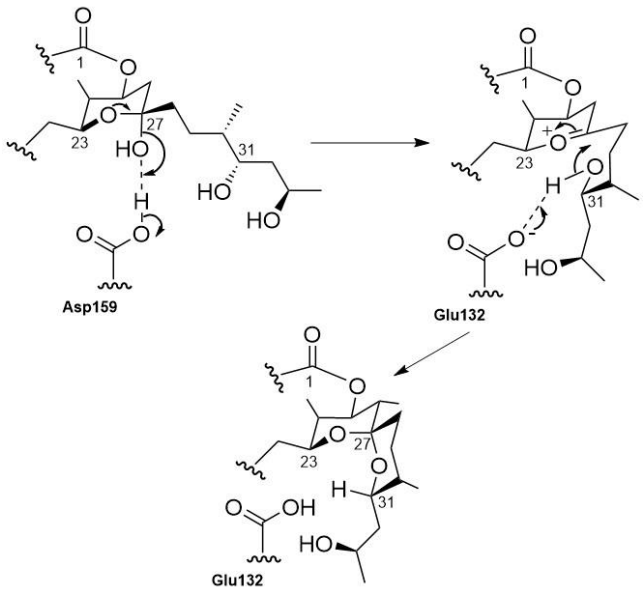

Figure 7. Mechanistic proposal for oligomycin acetal formation catalysed by spirocyclase OlmO. The 6,6-spiroacetal is formed by the interaction of the C-23- and C-31-hydroxyl groups with the C-27 keto group. The hemiacetal whose configuration is shown is assumed to form spontaneously and to be in equilibrium with other alternative hemiacetal forms and with the open-chain form. On binding to OlmO, loss of water from the hemiacetal, assisted by Asp159 acting as a general acid, generates an oxocarbenium ion which adopts a conformation in which the large sidechains are pseudoequatorial. The second acidic residue, Glu132, may then act as a general base to promote the attack of the C31-OH on the oxocarbenium ion to form the spiroacetal. In this thermodynamically favoured spiroacetal configuration, large substituents occupy equatorial positions and both oxygen atoms of the spiroacetal occupy an axial orientation with respect to the other ring, providing dual anomeric stabilization.

ASSOCIATED CONTENT

Experimental Section (materials, bacterial strains, and culture conditions; DNA isolation and manipulation; Metabolite analysis; Purification of the intermediates from *S. avermectinius* VL1001 *ΔolmO* mutant; Gene deletion in *S. avermectinius* VL1001 and *S. hygroscopicus* var. *ossamyceticus* DSM 40824; Complementation of *S. avermectinius* VL1001 *ΔolmO* mutant; Heterologous expression of *olmO* and *ossO* in *E. coli*. Protein quaternary structure analysis by analytical ultracentrifugation; In vitro assays; Protein crystallization and X-ray data collection and structure determination;) In-frame gene deletions of the spirocyclase genes; Non-enzymatic conversion of **3a** into **1a**; High-resolution mass analysis of **3a** and **3b**; ^{1}H NMR spectra of oligomycin A; ^{1}H-^{1}H COSY spectrum of compound **3a**. HSQC spectrum (one-bond ^{1}H-^{13}C correlation) of compound **3a**; HMBC spectrum (two and three-bond ^{1}H-^{13}C correlation) of compound **3a**.; Proposed structure for precursor **3a**; HPLC-MS analysis of the enzymatic conversion of **3a** (*m/z* 815.5280 $[M+Na]^{+}$) into **1a**; Multisequence alignment of OlmO and OssO with candidate spirocyclases; Quaternary structure of OlmO and OssO; Sequence alignment of OlmO and OssO; Superposition of OlmO and OssO; Dimerization interface of spirocyclases; Superposition of the structures of members of the calycin protein family; Analysis of active site volume of spirocyclases; Residues in the active site of spirocyclases; Analysis of molecular dinamic simulations; Assignment of the ^{13}C (125 MHz) and ^{1}H NMR (500 MHz) signals of oligomycin A (R=OH) **1b** and **3a**; Note on structure determination of **3a**; Crystallographic and model quality data statistics for OlmO and OssO; List of bacterial strains, plasmids and primers.

Supporting information is available free of charge at ..

AUTHOR INFORMATION

Corresponding Authors

*Dr. Oksana Bilyk - Department of Biochemistry, University of Cambridge, 80 Tennis Court Road, Cambridge, CB2 1GA, UK, e-mail: oksana.bilyk@recircle.com

*Dr. Marcio V. B. Dias - Department of Microbiology, Institute of Biomedical Science, University of Sao Paulo, Av. Prof. Lineu Prestes, 1374, CEP 05508-000, São Paulo, SP, Brazil, e-mail: mvb-dias@usp.br; and Department of Chemistry, University of Warwick, Coventry, CV47 7AL, UK.

Funding Sources

O.B. was supported by an EU Marie Skłodowska-Curie Fellowship (CaLiAT, project 705690). M.V.B.D. was supported by the São Paulo Research Foundation under grant 2018/00351-1 and 2020/03850-9 and CNPq 308998/2020-0. P.F.L. gratefully acknowledges the support of the Herchel Smith Chair of Biochemistry Fund, University of Cambridge.

Notes

PDB codes: The coordinates and structure factor files were deposited in the PDB with the following entries: 7SFN for OlmO and 7SFP for OssO;

The authors declare no competing financial interest.

ACKNOWLEDGMENT

We are grateful to Prof. Wen Liu (Shanghai Jiao Tong University) for sharing *S. avermectinius* VL1001 strain with us; Dr. Paul Brear for helping with protein crystallization and data collection and Dr. Katherine Stott for helping with the protein quaternary structure analysis.

REFERENCES

1. Staunton, J.; Weissman, K.J. Polyketide biosynthesis: a millennium review. *Nat. Prod. Rep.* **2001**, *18*, 380-416.
2. Hertweck, C. The biosynthetic logic of polyketide diversity. *Angew. Chem. Int. Ed. Engl.* **2009**, *48*, 4688-4716.
3. Kopp, F.; Marahiel, M.A. Where chemistry meets biology: the chemoenzymatic synthesis of nonribosomal peptides and polyketides. *Curr. Opin. Biotechnol.* **2007**, *18*, 513-520.
4. Olano, C., Mendez, C.; Salas, J.A. Post-PKS tailoring steps in natural product-producing actinomycetes from the perspective of combinatorial biosynthesis. *Nat. Prod. Rep.* **2010**, *27*, 571-616.
5. Pang, B.; Wang, M.; Liu, W. Cyclization of polyketides and non-ribosomal peptides on and off their assembly lines. *Nat. Prod. Rep.* **2016**, 33, 162-173.
6. Perron, F.; Albizati, K.F. Chemistry of Spiroketals. *Chem. Rev* **1989**, *89*, 1617 - 1661.
7. Aho, J.E., Pihko, P.M.; Rissa, T.K. Nonanomeric spiroketals in natural products: structures, sources, and synthetic strategies. *Chem. Rev.* **2005**, *105*, 4406-4440.
8. Zhang, F.M.; Zhang, S.Y.; Tu, Y.Q. Recent progress in the isolation, bioactivity, biosynthesis, and total synthesis of natural spiroketals. *Nat. Prod. Rep.* **2018**, *35*, 75-104.
9. Paterson, I.; Lam, N.Y.S. Challenges and discoveries in the total synthesis of complex polyketide natural products. *J. Antibiot.* **2018**, *71*, 215-233.
10. Takahashi, S.; Yasuyo, T.; Hiroshi, S.; Toshihiko, T.; Masakazu, N.; Ryuichiro, U.; Hiroyuki, Z.; Takuto, K.; Suresh, K.; Tohru, P.; Jun, D.; Haruo, I.; Sakaki, Y.; Osada, H. Reveromycin A biosynthesis uses RevG and RevJ for stereospecific spiroacetal formation. *Nat. Chem. Biol.* **2011**, *7*, 461-468.
11. Sun, P.; Zhao, Q.; Yu, F.; Zhang, H.; Wu, Z.; Wang, Y.; Wang, Y.; Zhang, Q.; Liu, W. Spiroketal formation and modification in avermectin biosynthesis involves a dual activity of AveC. *J. Am. Chem. Soc.* **2013**, *135*, 1540-1548.
12. Luhavaya, H.; Williams, S.R.; Hong, H.; Gonzaga de Oliveira, L.; Leadlay, P.F. Site-specific modification of the anticancer and antituberculosis polyether salinomycin by biosynthetic engineering. *Chembiochem* **2014**, *15*, 2081-2085.
13. Jiang, C.; Qi, Z.; Kang, Q.; Liu, J.; Jiang, M.; Bai, L.Formation of the Δ 18,19 double bond and bis(spiroacetal) in salinomycin is atypically catalyzed by SlnM, a methyltransferase-like enzyme. *Angew. Chem. Int. Ed. Engl.* **2015**, *54*, 9097-9100.
14. Bilyk, O.; Samborskyy, M.; Leadlay, P.F. The biosynthetic pathway to ossamycin, a macrocyclic polyketide bearing a spiroacetal moiety. *PLoS One* **2019**, *14*, e0215958.
15. Õmura, S.; Ikeda, H.; Ishikawa, J.; Hanamoto, A.; Takahashi, C.; Shinose, M.; Takahashi, Y.; Horikawa, H.; Nakazawa, H.; Osonoe, T.; Kikuchi, H.; Shiba, T.; Sakaki, Y.; Hattori, M. Genome sequence of an industrial microorganism Streptomyces avermitilis: deducing the ability of producing secondary metabolites. *Proc. Natl. Acad. Sci. U. S. A.* **2001**, *98*, 12215-12220.
16. Sun, Y.; He, X.; Liang, J.; Zhou, X.; Deng, Z. Analysis of functions in plasmid pHZ1358 influencing its genetic and structural stability in *Streptomyces lividans* 1326. *Appl. Microbiol. Biotechnol.* **2009**, *82*, 303-310.
17. Camacho, C.; Coulouris, G.; Avagyan, V.; Ma, N.; Papadopoulos, J.; Bealer, K.; Madden, T.L. BLAST+: architecture and applications. *BMC Bioinformatics*, **2009,** 10, 421.
18. Larkin, M.A.; Blackshields, G.; Brown, N.P.; Chenna, R.; McGettigan, P.A.; McWilliam, H.; Valentin, F.; Wallace, I.M.; Wilm, A.; Lopez, R.; Thompson, J.D.; Gibson, T.J.; Higgins, D.G. Clustal W and Clustal X version 2.0. *Bioinformatics* **2007**, *23*, 2947-2948).
19. Kumar, S., Stecher, G.; Tamura, K. MEGA7: Molecular Evolutionary Genetics Analysis Version 7.0 for Bigger Datasets. *Mol. Biol. Evol.* **2016,** *33*, 1870-1874.
20. Schaffert, L.; Albersmeier, A.; Winkler, A.; Kalinowski, J.; Zotchev, S.B.; Rückert, C. Complete genome sequence of the actinomycete Actinoalloteichus hymeniacidonis type strain HPA 177(T) isolated from a marine sponge. *Stand Genomic Sci.* **2016**, **11**, 91.
21. Sato, S., Iwata, F., Yamada, S.; Katayama, M. Neomaclafungins A-I: oligomycin-class macrolides from a marine-derived actinomycete. *J. Nat. Prod.* **2012**, **75**, 1974-1982.
22. Harvey, B.M.; Mironenko, T.; Sun, Y.; Hong, H.; Deng, Z.; Leadlay, P.F.; Weissman, K.J.; Haydock, S.F.Insights into polyether biosynthesis from analysis of the nigericin biosynthetic gene cluster in Streptomyces sp. DSM4137. *Chem. Biol.* **2007**, **14**, 703-714.
23. Liu, R.; Fang, F.; An, Z., Huang, R.; Wang, Y.; Sun, X.; Fu, S.; Fu, A.; Deng, Z.; Liu, T. Genomics-driven discovery of the biosynthetic gene cluster of maduramicin and its overproduction in Actinomadura sp. J1-007. *J. Ind. Microbiol. Biotechnol.* **2020**, *47*, 275-285.
24. Oja, T.; Palmu, K.; Lehmussola, H.; Leppäranta, O.; Hännikäinen, K.; Niemi, J.; Mäntsälä, P.; Metsä-Ketelä, M. Characterization of the alnumycin gene cluster reveals unusual gene products for pyran ring formation and dioxan biosynthesis. *Chem. Biol.* **2008**, *15*, 1046-1057.
25. Oja, T.; Klika, D.; Appassamy, L.; Sinkkonen, J.; Mäntsälä, P.; Niemi, J.; Metsä-Ketelä, M. Biosynthetic pathway toward carbohydrate-like moieties of alnumycins contains unusual steps for C-C bond formation and cleavage. *Proc. Natl. Acad. Sci. U. S. A.* **2012**, *109*, 6024-6029.
26. Miyanaga, A. Michael additions in polyketide biosynthesis. *Nat. Prod. Rep.* **2019**, *36*, 531-547.
27. Wu, Q.; Liang, J.; Lin, S.; Zhou, X.; Bai, L.; Deng, Z.; Wang, Z. Characterization of the biosynthesis gene cluster for the pyrrole polyether antibiotic calcimycin (A23187) in S*treptomyces chartreusis* NRRL 3882. *Antimicrob. Agents Chemother.* **2011**, *55*, 974-982.
28. Young, J.; Taylor, R.E. Evolution of polyketides: post-PKS processing in the formation of spiroketals. *Nat. Prod. Rep.* **2008**, *25*, 651-655.
29. Davis, I.W.; Leaver-Fay, A.; Chen, V.B.; Block, J.M.; Karpal, G.J.; Wang, X.; Murray, L.W.; Arendall, W.B.; Snoeyink, J.; Richardson, J.S.; Richardson, D.C. MolProbity: all-atom contacts and structure validation for proteins and nucleic acids. *Nucleic Acids Res.* **2007**, *35*, W375-383.
30. Holm, L.; Laakso, L.M. Dali server update. *Nucleic Acids Res.* **2016**, *44*, W351-355.
31. Flower, D.R., North, A.C.; Sansom, C.E. The lipocalin protein family: structural and sequence overview. *Biochim. Biophys. Acta* **2000**, *1482*, 9-24.
32. Flower, D.R., North, A.C.; Attwood, T.K. Structure and sequence relationships in the lipocalins and related proteins. *Protein Sci.* **1993**, *2*, 753-761.
33. Lim, S.M.; Chen, D.; Teo, H.; Roos, A.; Jansson, A.E.; Nyman, T.; Trésaugues, L.; Pervushin, K.; Nordlund, P. Structural and

dynamic insights into substrate binding and catalysis of human lipocalin prostaglandin D synthase. *J. Lipid Res.* **2013**, *54*, 1630-1642.

34. Tian, W.; Chen, C.; Lei, X.; Zhao, J.; Liang, J. CASTp 3.0: computed atlas of surface topography of proteins. *Nucleic Acids Res* 2018, *46*, W363-W367 (2018).

35. T. Kumasaka, K. Aritake, H. Ago, D. Irikuma, T. Tsuruuma, M. Yamamato, M. Miyano, Y. Urade, O. Hayaishi, Structural basis of the catalytic mechanism operating in open-closed conformers of lipocalin type prostaglandin D synthase. *J. Biol. Chem.* **2009**, *284*, 22344-22352.

Table of Contents

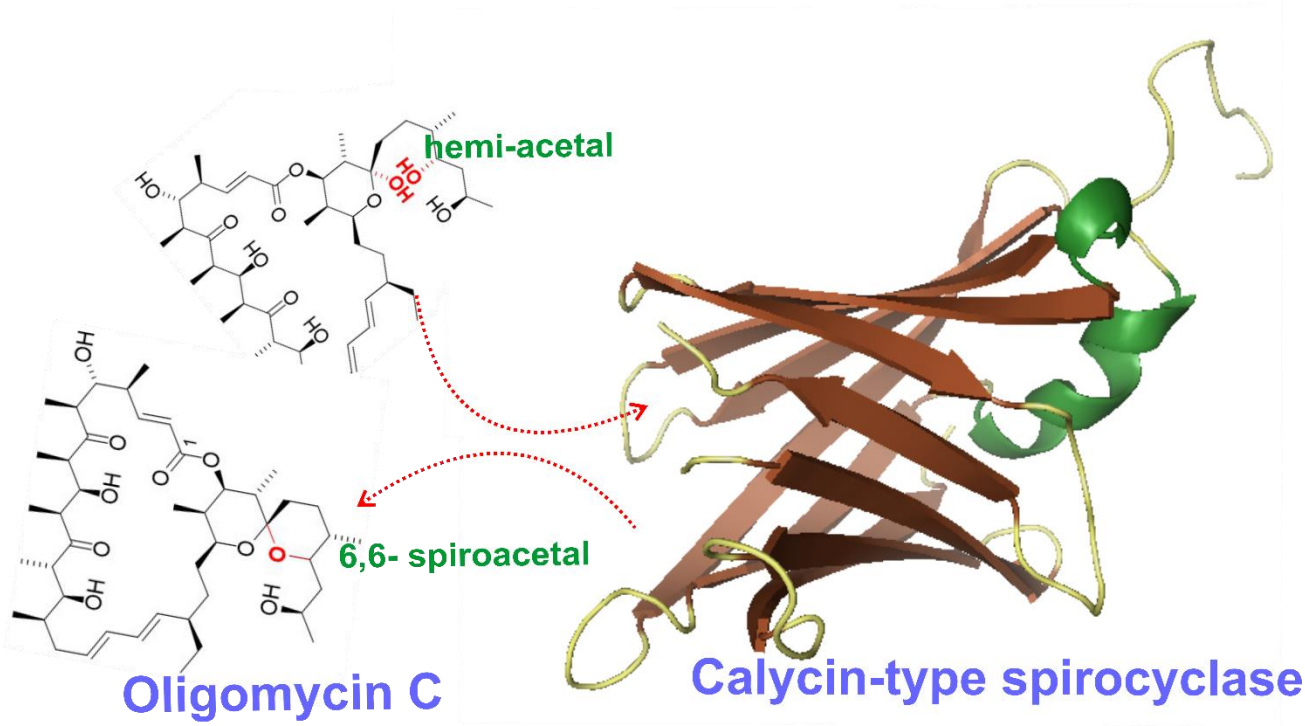

The formation of the spiroacetal ring systems in oligomycin and ossamycin was found to involve an unprecedented spirocyclase (OlmO and OssO, respectively). The crystal structures of these enzymes show an unusual β-barrel similar to those from the calycin protein family. Three charged amino acid residues clustered together in the lumen of the barrel were confirmed to be involved in the spirocyclase activity.